Journal of the Chinese Society of Mechanical Engineers, Vol.47, No.1, pp 129~138 (2026)

High-Speed Robotic Manipulator Vibration Control via B-Spline Trajectory Generation and L-BFGS-B Optimization

Peng-Jen Chen[*,**], Ta-Jen Peng[**,***], Ching-Li Liu[****] and En-Cheng Liou[****]

Keywords: High-speed robotic arm, trajectory planning, vibration suppression , robotic control

ABSTRACT

High-speed robotic operations often generate significant vibrations and trajectory deviations, compromising precision and efficiency in industrial automation. This study proposes an advanced motion control strategy integrating B-Spline trajectory planning with the L-BFGS-B optimization algorithm and systematic tuning of CNT and Override parameters. Experimental validation involved a six-axis robotic arm executing a standard 90-degree corner path and a complex multi-turn trajectory. Results indicate optimal parameter tuning effectively balances vibration suppression and positional accuracy, maintaining vibration magnitudes between 0.75 and 1.25 G. Utilizing two B-Spline control points significantly reduces average positional error from 27.68 mm to 7.52 mm, with a minimal operation time increase of 0.15 seconds. Compared to conventional methods, the proposed approach achieves a 12% reduction in execution time and a 35% reduction in positional errors, highlighting its efficacy and substantial potential to enhance automated manufacturing systems, precision machining tasks, and advanced robotic motion planning applications.

Paper Received March, 2025. Revised April, 2025. Accepted May, 2025. Author for Correspondence: Ta-Jen Peng.

[*]*Associate Professor, Department of Intelligent Automation Engineering, National Chin-Yi University of Technology, Taiwan 411030 R.O.C.*

[**]*Hydrogen and Fuel Cells Sustainable Development Center, Taiwan 411030 R.O.C.*

[***]*Asscoiat Professor, Department of Intelligent Automation Engineering, National Chin-Yi University of Technology, Taiwan 411030 R.O.C.*

[****]*Undergraduate Student, Department of Intelligent Automation Engineering, National Chin-Yi University of Technology, Taiwan 411030 R.O.C.*

INTRODUCTION

With the rapid advancement of Industry 4.0 and smart manufacturing technologies, robotic manipulators have increasingly become essential components in modern production processes. In particular, robotic arms play pivotal roles in high-precision and high-stability tasks such as spraying, welding, and high-speed assembly operations, making them core technologies in automated manufacturing systems (Wang et al., 2023; Dzedzickis et al., 2021). For instance, automotive welding processes require precise control of weld spot positions to avoid defects caused by vibrations or unstable movements. Similarly, precise spray coating operations in consumer electronics demand stable and uniform robotic arm trajectories to maintain product quality (Hong et al., 2014; Kiran & Prabhu, 2020). Furthermore, as quality requirements in electronics, semiconductor manufacturing, and precision machinery industries continue to rise, demands for higher precision and stability in robotic arm motion control are correspondingly increasing. Consequently, achieving high accuracy in trajectory control and effective vibration suppression under high-speed conditions has emerged as a critical challenge in the industrial sector (Gasparetto & Zanotto, 2010; Wang et al., 2023).

However, frequent acceleration and deceleration during high-speed operations often induce vibrations and trajectory distortions in robotic manipulators, degrading product surface quality and increasing equipment wear and operational costs (Soori et al., 2023; Uzuner et al., 2017; Park & Asada, 1994). Additionally, these distortions and vibrations may accelerate mechanical fatigue, adversely affecting production efficiency and maintenance costs (Zhang et al., 2021; Abe, 2016). Therefore, effectively balancing stability and precision during high-speed robotic motion has become a fundamental research issue in robotic motion control (He et al., 2023; Ratiu & Prichici, 2017).

Currently, two mainstream control modes are predominantly adopted in industrial settings: point-to-point (FINE) and continuous motion (CNT). Each method has inherent limitations. The FINE mode, although precise in positioning, generates significant vibrations due to abrupt acceleration changes at high speeds. Conversely, the CNT mode effectively reduces vibrations but fails to achieve desired trajectory precision in complex or high-accuracy applications (Ziaukas et al., 2017; He et al., 2020; Lewis et al., 2003). As a result, curve-based trajectory generation methods aiming to balance smoothness and positional accuracy have garnered increased research attention (Wang et al., 2019; Biagiotti et al., 2019; Fang et al., 2019). Among these approaches, B-Spline curves offer superior flexibility by adjusting the number of control points and the order of basis functions to accommodate diverse motion conditions, emerging as a predominant method for trajectory planning in industrial robotic arms (Huo et al., 2024; Eshtehardian & Khodaygan, 2023; Zeng & Wang, 2025; Lu et al., 2021).

Several studies have demonstrated that applying B-Spline curves to industrial robotic manipulators effectively enhances trajectory smoothness and reduces vibration amplitude. For example, Wang et al. (2023) and Uzuner et al. (2017) successfully utilized B-Spline methods to significantly improve trajectory smoothness and accuracy. Similarly, Huo et al. (2024), Eshtehardian & Khodaygan (2023), Zeng & Wang (2025), and Lu et al. (2021) demonstrated the practical effectiveness of B-Spline curves in achieving smoother trajectories in precision robotic operations.

Moreover, optimization algorithms such as particle swarm optimization (Ekrem & Aksoy, 2023), genetic algorithms (Lamini et al., 2018), and differential evolution algorithms (Juříček et al., 2023) have been integrated with B-Spline methods to further enhance robotic performance. Nevertheless, most existing studies focus primarily on static or low-speed scenarios, with limited research addressing trajectory distortion and vibration control under high-speed conditions. Additionally, traditional high-speed motion control methods often require extensive experimentation and tuning, which are time-consuming and seldom yield optimal results (Yamakawa et al., 2010; Gasparetto et al., 2015). Thus, employing advanced numerical optimization techniques for automatic adjustment of motion parameters and control points has become a significant research direction.

This study introduces an innovative motion control strategy integrating B-Spline trajectory generation with the L-BFGS-B optimization algorithm. The objective is to effectively reduce vibration and trajectory errors in high-speed dynamic operations through optimal control point adjustments. By comparing the proposed approach with traditional FINE and CNT methods, this research seeks to offer a more effective solution for high-speed, high-precision robotic manipulator control. The findings are expected to contribute significantly to the fields of automated manufacturing, robotic trajectory planning, and related industrial developments.

THEORETICAL METHODOLOGY

To address vibration and trajectory distortion problems experienced by robotic manipulators operating at high speeds, this study proposes an integrated motion control strategy combining point-to-point (FINE), continuous (CNT) control modes, and B-Spline curve generation methods. The core concept involves selecting an appropriate control mode flexibly based on specific motion requirements and leveraging the smoothness of B-Spline curves to generate ideal motion trajectories. Additionally, the L-BFGS-B optimization algorithm is employed to optimize trajectories, further enhancing the overall performance of robotic manipulators.

Traditional control modes (FINE and CNT)

The Fine Interpolation (FINE) mode utilizes fixed acceleration and deceleration profiles, allowing robotic manipulators to achieve rapid and precise point-to-point positioning. While suitable for low-speed, high-precision tasks, this mode can generate significant vibrations and equipment wear under high-speed conditions due to abrupt acceleration changes. Conversely, the Continuous Motion (CNT) mode emphasizes smooth motion transitions and velocity continuity, effectively reducing vibration. However, CNT mode relies on linear segments with fixed curvature designs, making it challenging to completely eliminate trajectory deviations and positional errors in high-speed, complex trajectories.

The core calculation of the CNT control mode is defined as

$$a = \frac{\Delta v}{\Delta t} \times \left(1 - \frac{CNT}{100}\right) \quad (1)$$

where Δv represents is the velocity variation, Δt is the time interval, and the CNT parameter ranges from 0 to 100, indicating the degree of motion continuity. Higher CNT values result in smoother acceleration and deceleration profiles, but may decrease positional accuracy. Nevertheless, CNT mode still exhibits trajectory deviation and positioning errors in high-speed, complex path scenarios.

B-Spline curve generation

B-Spline (Basis Spline) curves, widely used in trajectory planning, offer high smoothness and flexibility suitable for high-speed and continuously smooth robotic manipulator motion planning. Compared to FINE and CNT modes, B-Spline curves

provide increased degrees of freedom in trajectory design, effectively managing trajectory curvature and significantly reducing vibrations and positional errors at high speeds.

The basic formulation of a B-Spline curve is expressed as:

$$C(u) = \sum_{i=0}^{n} N_{i,k}(u) \cdot P_i \quad (2)$$

where $C(u)$ represents the position of the curve at the parameter (u), Pi denotes the control point coordinates, and $N_{i,k}(u)$ is the k th basis function corresponding to the i th control point. The B-Spline basis function $N_{i,k}(u)$ is defined recursively as follows:

1. When k=0, the basic function is

$$N_{i,0}(u) = \begin{cases} 1, & t_i \le u < t_{i+1} \\ 0, & otherwise \end{cases} \quad (3)$$

2. When k>0, the basic function is

$$N_{i,k}(u) = \frac{u - t_i}{t_i + k - t_i} N_{i,k-1}(u) + \frac{t_i + k + 1 - u}{t_i + k + 1 - t_i + 1} N_i + 1, k - 1(u) \quad (4)$$

where t_i is the knot vector determining the influence range of each control point. By adjusting knot vectors and the number of control points, B-Spline curves can ensure smooth transitions in trajectories and effectively reduce vibrations during high-speed movements.

Optimization using the L-BFGS-B algorithm

To further enhance the effectiveness of B-Spline curve trajectory planning, this study employs the Limited-memory Broyden–Fletcher–Goldfarb–Shanno with Box constraints (L-BFGS-B) optimization algorithm to optimize control point placement. L-BFGS-B is a quasi-Newton optimization method well-suited for large-scale problems with or without boundary constraints. It significantly reduces computation and storage costs by using a low-rank approximation of the Hessian matrix, thereby making it particularly suitable for handling high-dimensional problems and widely effective in solving practical multidimensional parameter optimization issues.

The fundamental steps of the L-BFGS-B algorithm are outlined as follows:

(1) **Initialization:** set initial point x_0 and initial Hessian approximation matrix B_k

(2) **Compute search direction:** at iteration k, determine the descent direction p_k by solving:

$$B_k \cdot p_k = -\nabla f(x_k) \quad (5)$$

where $\nabla f(x_k)$ represents the gradient at point x_k.

(3) **Line Search:** perform a line search along direction p_k to determine an appropriate stepsize α_k, updating position as:

$$x_{\{k+1\}} = x_k + \alpha_k \cdot p_k \quad (6)$$

where α_k is chosen to satisfy sufficient decrease and curvature conditions.

(4) **Variable update:** define the following difference vectors before updating the Hessian approximation:

$$y_k = \nabla f\left(x_{\{k+1\}}\right) - \nabla f(x_k) \quad (7)$$

where $s_k = x_{\{k+1\}} - x_k$ and each term enforces the quasi-Newton secant condition and maintains symmetric positive definiteness of the approximation. This vector s_k is crucial in updating the Hessian approximation matrix, as it contains information regarding the step direction and magnitude of parameter changes during each iteration.

(5) **Update Hessian Approximation:** update the Hessian matrix approximation using:

$$B_{\{k+1\}} = B_k + \frac{(y_k \cdot y_k^T)}{(y_k^T \cdot s_k)} - \frac{(B_k \cdot s_k \cdot s_k^T \cdot B_k^T)}{(s_k^T \cdot B_k \cdot s_k)} \quad (8)$$

The optimization objective function used in this research is defined as:

$$f = \alpha A + \beta D + \gamma T \quad (9)$$

where α, β and γ are weighting coefficients balancing the requirements of vibration suppression (A), positioning accuracy (D), and motion efficiency (T). The optimized curve aims to achieve the optimal trade-off among these three factors.

As shown in Figure 1, the two iterative curves represent the respective variations of two generated control points during the B-Spline optimization process. In the early stages, the L-BFGS-B algorithm demonstrated rapid convergence within the first six iterations, during which the control point positions underwent significant adjustments to seek an optimal configuration. Starting from the seventh iteration, the magnitude of changes in control point positions gradually decreased, indicating that the algorithm was approaching a global optimum. Between the seventh and nineteenth iterations, the convergence trend stabilized, with only minor adjustments observed to confirm the solution's stability. Convergence was successfully achieved by the nineteenth iteration, further validating the efficiency and robustness of the L-BFGS-B algorithm in optimizing B-Spline control points.

Notably, the two curves exhibit highly similar convergence behavior. This can be attributed to the geometric similarity of the roles these control points play in the shape of the curve, as well as the symmetric nature of their initial configurations. As a result, their update directions and magnitudes during the gradient descent process of the error function were closely aligned. This phenomenon reflects the strong interdependence between control points and demonstrates the L-BFGS-B algorithm's capability to preserve the overall structural characteristics of the curve while simultaneously optimizing the positions of related control points.

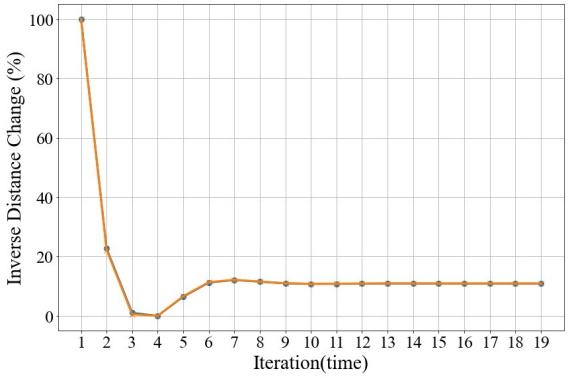

Fig. 1. Convergence curve illustrating the optimization process using the L-BFGS-B algorithm.

The vertical axis represents the rate of change in the inverse of the distance between control points over two consecutive iterations. Denote the actual distance at the ith iteration as d_i, then the inverse distance is $\frac{1}{d_i}$, which is used to measure the relative change between two iterations. Inverse distance change (IDC) is defined as:

$$\text{IDC} = \mathbf{100}\% \times \left| \frac{\frac{1}{d_i} - \frac{1}{d_{i-1}}}{\frac{1}{d_{i-1}}} \right| \qquad (10)$$

In this Fig 1, the vertical axis represents the inverse of distance. The change of approximately 10% can be observed in later iterations, and the measured data indicate that the maximum displacement of the control points between adjacent iterations is about 0.00066 mm. This correspondingly minute actual displacement suggests that the algorithm has nearly converged.

EXPERIMENTAL DESIGN AND METHODOLOGY

This study investigates the integration of B-Spline trajectory generation methods with robotic manipulator motion control, specifically focusing on curvature adjustments to mitigate vibration and trajectory distortion during high-speed operations. Experiments were systematically structured into three sequential phases. In the first phase, various combinations of CNT and Override parameters were evaluated using a standardized 90° corner path (Figure 2), emulating typical high-speed cornering conditions. Metrics such as vibration amplitude, average vibration levels, and dominant vibration frequencies were recorded to identify the optimal parameter settings for reducing vibrations and enhancing system efficiency.

In the second phase, the optimal parameters determined previously were applied to assess how variations in B-Spline control point quantity influenced vibration amplitude and trajectory smoothness. Control point numbers ranging incrementally from two to ten were systematically evaluated to identify the mınimal number required for achieving optimal trajectory performance without excessive computational complexity.

The final phase involved validating the optimized parameters and B-Spline trajectory against traditional FINE and CNT motion modes through a more complex, multi-turn trajectory, representative of realistic high-speed operations. Comparative analyses of vibration amplitude, trajectory deviation, and execution time confirmed the practical efficacy and superior performance of the optimized B-Spline approach.

Experiments were conducted using a FANUC ROBOT M-20iD/25 manipulator (Figure 3 (a)), featuring a six-axis joint structure, a rated payload of 25 kg, and repeatability accuracy of ±0.02 mm. To enhance vibration measurement sensitivity, a triaxial ICP® accelerometer (PCB Piezotronics Model 356A32; sensitivity: 100 mV/g ±10%, frequency response: 1 Hz–4 kHz, measurement range: ±50 g pk) was securely mounted at the distal end of a 30 cm aluminum extension rail attached to the manipulator's end-effector via a rigid 3 mm thick L-shaped steel bracket (Fig. 3 (b)). Vibration signals were captured using a CompactDAQ USB chassis (NI/Emerson Model cDAQ-9174) equipped with a NI-9234 Sound & Vibration input module (4-channel, 24-bit resolution, IEPE compatible). Signals were sampled continuously at rates exceeding 10 kHz and transmitted to a control computer for real-time analysis and recording (Fig. 3 (c)).

Real-time vibration data processing involved Fast Fourier Transform (FFT) analysis configured within a frequency bandwidth from 0 Hz to 2 kHz, with frequency resolution set at 50 lines (ΔF = 40 Hz) and data block size of 128 samples (0.025 s window). Zoom FFT functionality was disabled, and a custom envelope filter without specific frequency band limitations was applied. Comprehensive RMS values covering 0–2000 Hz were computed for thorough spectral analysis of dynamic behaviors. Prior to experiments, strict calibration procedures for the accelerometer and data acquisition system were implemented under controlled environmental and mounting conditions, ensuring measurement accuracy and repeatability throughout the experimental process.

Phase 1: CNT and override parameter combination tests

In this phase, the manipulator executed a predefined 90-degree corner path (Fig. 2). CNT and Override parameters were systematically varied to record stability, vibration amplitude, execution time, and operational efficiency. The manipulator was controlled to operate consistently at stable speeds, with synchronized data collection to analyze and

determine the optimal parameter set that achieves the best balance between vibration suppression and high efficiency.

Phase 2: B-Spline curvature adjustment

After determining the optimal CNT and Override parameters, the number of B-Spline control points was varied from two to ten. For each control point configuration, vibration amplitudes and trajectory smoothness were measured and compared. The optimal configuration was identified based on minimal vibration amplitudes while maintaining optimal trajectory smoothness.

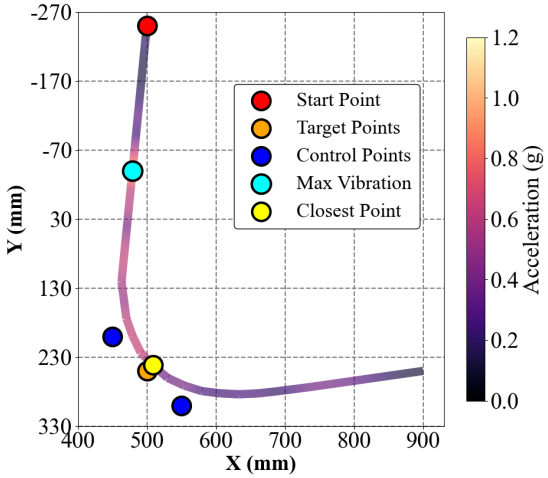

Fig. 2. Schematic diagram of the fixed 90-degree manipulator trajectory.

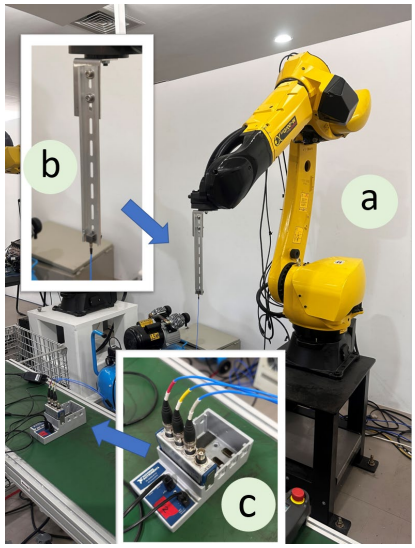

Fig. 3. Experimental setup: (a) FANUC ROBOT M-20iD/25 manipulator and test posture; (b) accelerometer installation location; (c) data acquisition device.

Phase 3: Validation of optimized parameter scheme

This phase employed a more complex trajectory to simulate realistic dynamic environments. The optimized B-Spline curvature adjustment and parameter set were compared against traditional FINE and CNT methods by recording vibrations, trajectory deviations, and execution times for each method. Comparative analyses validated the effectiveness of the optimized approach under complex motion path scenarios.

RESULTS AND DISCUSSION

Impact of CNT and override parameters on vibration and trajectory accuracy

This study first analyzed the impact of different CNT and Override parameter combinations on vibrations and trajectory accuracy under high-speed conditions. The experimental results (Figure 4 to 7) indicate that, for a fixed 90-degree corner path, variations in CNT and Override parameters produced generally similar vibration trajectories but significantly different vibration amplitudes and energy distributions. Particularly, combinations with lower CNT values and higher Override values (e.g., CNT5 + Override70) exhibited noticeably concentrated vibrations.

Further comparison of maximum vibration and positional deviation under various CNT settings at fixed execution time was conducted. The execution time was fixed by adjusting the Override parameter, the maximum vibration and positional deviation under different CNT settings were compared (as shown in Fig. 5). The horizontal axis represents different parameter configurations, while the vertical axis displays both the maximum vibration and the minimum distance between the measured points and the robotic manipulator's ideal trajectory. Results indicate that under identical execution time conditions, higher CNT settings gradually reduced maximum vibration amplitude (decreasing from approximately 0.12 G to 0.07 G). However, positional deviation significantly increased (rising from approximately 2 mm to 51 mm), demonstrating that while increasing CNT values effectively mitigates vibration, it simultaneously compromises positional accuracy. This reveals a clear trade-off between these parameters, necessitating adjustment of CNT settings based on specific application requirements to balance vibration suppression and positional precision.

Fig. 6 compares maximum vibration power, maximum positional deviation, and execution times for different CNT settings under a fixed Override condition. A nonlinear relationship was observed, with the CNT50 setting exhibiting relatively better performance, showing lower maximum vibration power and positional deviation.

An analysis of average vibration amplitudes (RMS values) under various CNT conditions (Figure. 8) revealed minimal fluctuations across CNT settings,

with RMS values consistently ranging between 0.2 and 0.3 G. This indicates that variations in CNT parameters have limited effects on average vibration amplitudes, emphasizing the stability of CNT parameter adjustments for high-speed motion control.

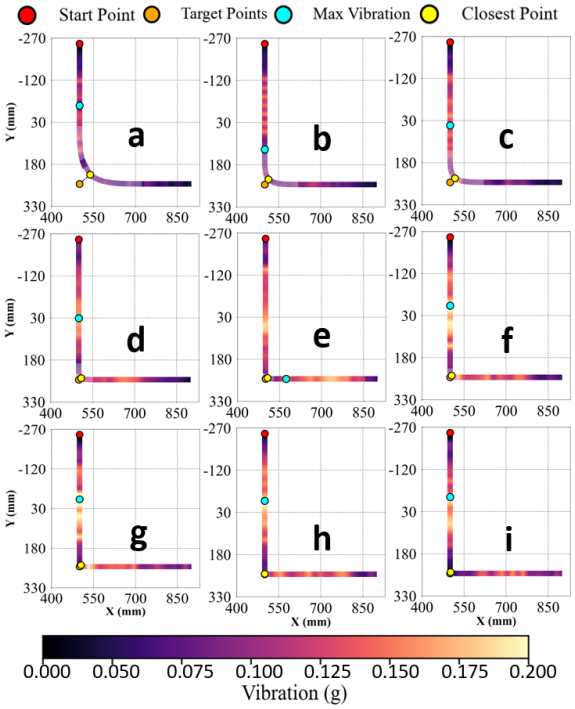

Fig. 4. Maximum vibration power and maximum positional deviation corresponding to each parameter set:(a) OVERRIDE40% CNT100, (b) OVERRIDE 45% CNT75, (c) OVERRIDE 50% CNT50, (d) 65% CNT25, (e) OVERRIDE 65% CNT15, (f) OVERRIDE 70% CNT10, (g) OVERRIDE 70% CNT5, (h) OVERRIDE 70% CNT1, (i) OVERRIDE 70% CNT0.

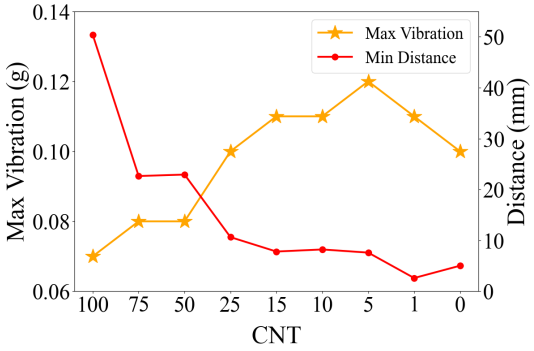

Fig. 5. Comparison of maximum vibration and position deviation for different CNT under a fixed-time parameter combination

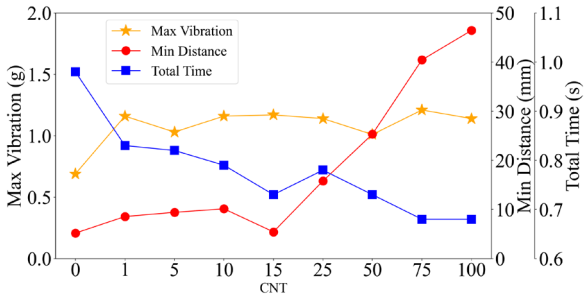

Fig. 6. Comparison of maximum vibration, minimum positional deviation, and total execution time under various CNT settings.

Influence of b-spline control point quantity on motion performance

B-Spline curves, known for their smooth and differentiable nature, are widely applied in automated path planning. To further enhance trajectory accuracy and motion performance, this study evaluated the impact of control point quantity on B-Spline trajectory planning, optimizing control point positions using the L-BFGS-B algorithm. Experiments were conducted with three configurations: no control points, two control points, and three control points, examining trajectory precision, vibration characteristics, and total execution times comprehensively.

Experiments proceeded according to the following steps: first, a specified number of control points were inserted into the B-Spline curve. Next, the L-BFGS-B algorithm optimized the positions of these control points. Finally, trajectory tracking tests were conducted under various CNT conditions, measuring total execution time, average vibration, maximum vibration, and control point positional errors. Experimental results (Figure 7 to 10) indicated that trajectory accuracy was poorest without control points (average deviation of 27.68 mm), significantly improved with two control points (7.52 mm), but worsened with three control points (17.09 mm), suggesting that excessive control points may lead to overfitting, thus reducing system efficiency. Regarding vibration performance, average vibrations exhibited minimal differences across different control point numbers, implying limited effects of increased control points on average vibration control.

However, the maximum vibration was reduced to 0.512 g in some cases with three control points, better than other configurations (approximately 0.95 to 0.976 g), though insufficient to offset accuracy losses. Execution time was shortest with no control points (0.768 s), but accuracy was lowest. The two control points configuration increased execution time slightly (0.916 s on average), achieving an optimal balance among accuracy, vibration, and efficiency. The three control points configuration further increased execution time (0.944 s) without evident overall

benefits. Thus, this study concludes that a moderate number of control points effectively improves trajectory accuracy, with two control points providing the best performance balance for high-speed control applications. Future research may explore adaptive weight adjustment mechanisms to dynamically balance accuracy, vibration, and execution time for different operational demands.

Validation of optimized parameter scheme on complex trajectories

To evaluate the practical effectiveness of the optimized parameter scheme proposed in this study, a complex trajectory characterized by multiple curves and turns was designed. A quantitative comparative analysis was conducted among the traditional FINE mode, CNT mode, and the optimized mode proposed herein, referred to as the "B-Spline with L-BFGS-B optimization" mode (abbreviated as the optimized mode hereafter)

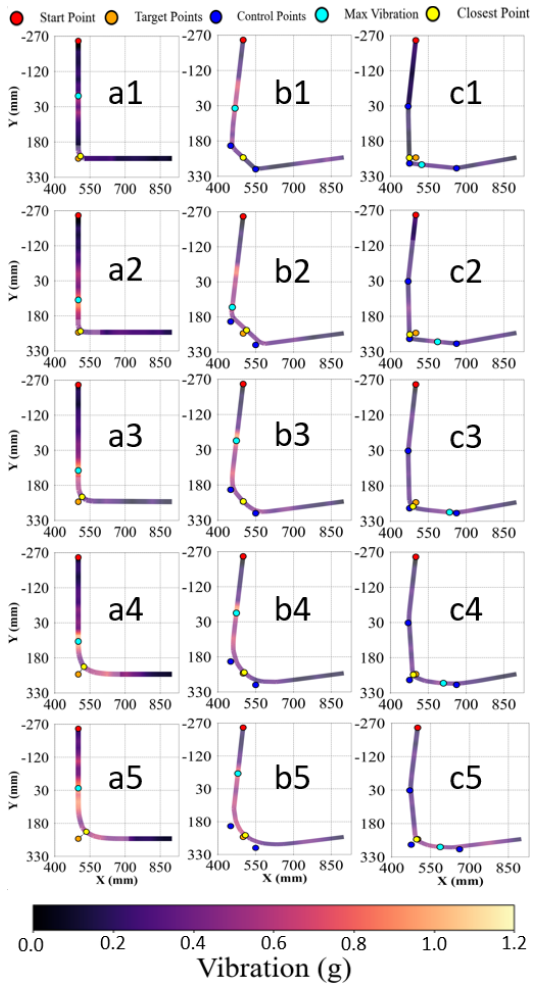

Fig. 7. Compares vibration amplitude distributions under various control point quantities and CNT settings:(a1)-(a5) No control points, CNT 100, CNT 75, CNT 50, CNT 25, CNT 0;(b1)-(b5) Two control points, CNT 100, CNT 75, CNT 50, CNT 25, CNT 0;(c1)-(c5) Three control points, CNT 100, CNT 75, CNT 50, CNT 25, CNT 0.

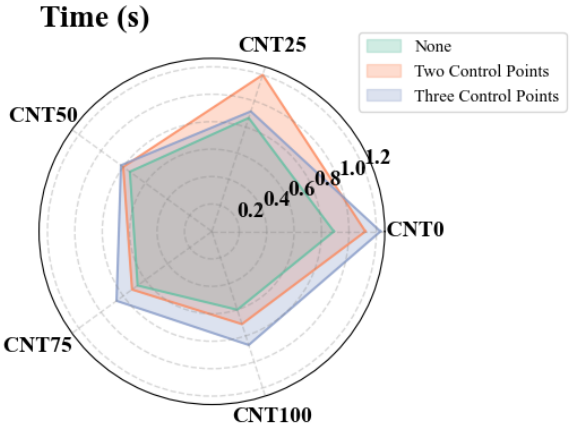

Fig. 8. Compares total execution time under various control point quantities and CNT settings.

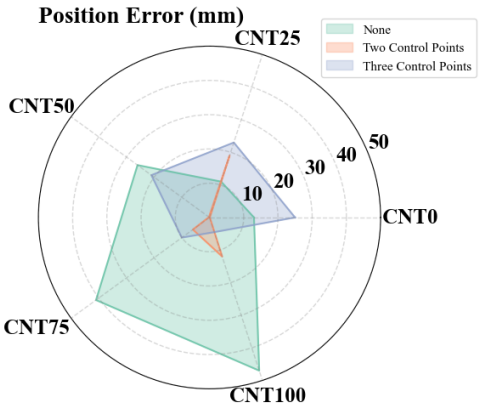

Fig. 9. Comparison of positional deviations under varying numbers of control points and CNT settings.

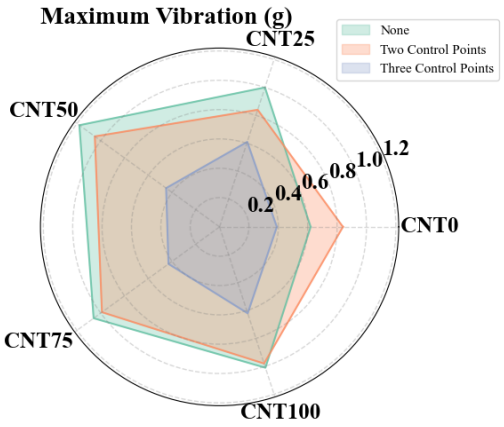

Fig. 10. Comparison of maximum vibrations under varying numbers of control points and CNT settings.

The experimental results, presented in Figure 11 and 12, demonstrate that under various CNT settings, the optimized mode achieved an average reduction in

total execution time of approximately 12% compared to traditional FINE and CNT modes. Additionally, positional deviation was reduced by about 35%, and vibration differences were decreased by approximately 20%. Notably, under higher CNT settings (such as CNT75 and CNT100), the optimized mode reached total execution times around 0.75 seconds, with positional deviations effectively controlled within 5 mm, representing a significant performance improvement over non-optimized modes.

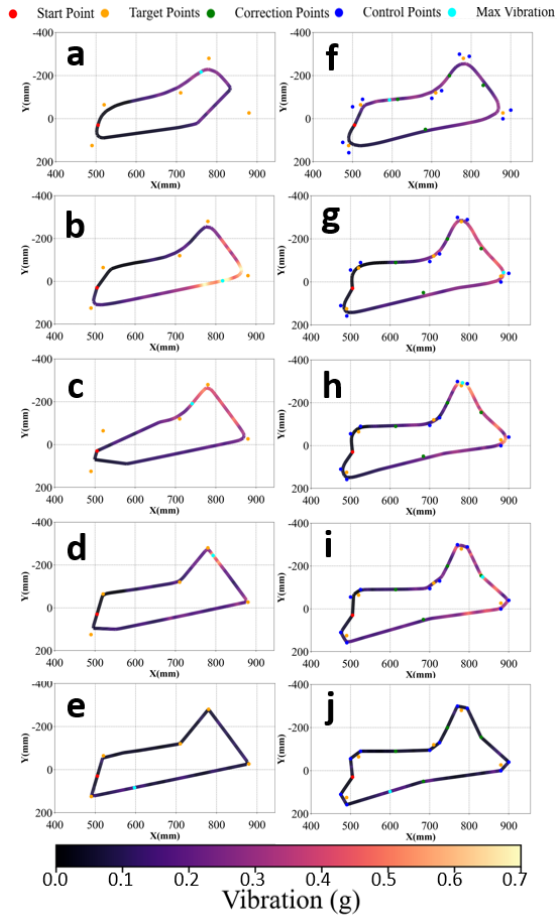

Fig. 11. Comparison of vibration differences between the non-optimized and optimized methods under various CNT settings for complex trajectories:(a) Non-optimized mode, CNT 100, (b) Non-optimized mode CNT 75, (c) Non-optimized mode CNT 50, (d) Non-optimized mode CNT 25, (e) Non-optimized mode CNT 0, (f) Optimized mode CNT 100, (g) Optimized mode CNT 75, (h) Optimized mode CNT 50, (i) Optimized mode CNT 25, (j) Optimized mode CNT 0.

Although the vibration level in the optimized mode was slightly higher than in the non-optimized modes, it remained within acceptable limits (approximately 0.8 to 1.0 G). Moreover, the enhancements in positional accuracy and execution time notably improved the overall system performance, making this optimized method especially suitable for high-speed industrial applications with stringent accuracy requirements. Based on these quantitative analyses, the optimized mode not only effectively manages complex, high-speed trajectories but also exhibits superior precision control and efficiency improvements, verifying its practicality and reliability in industrial settings.

Further comparative analysis is illustrated in Fig. 11, clearly showing the differences between optimized and non-optimized modes when executing the complex trajectory. Fig. 12 presents trajectory profiles under various CNT settings (CNT100, CNT75, CNT50, CNT25, CNT0) for both non-optimized and optimized modes. It is distinctly observed from these figures that, under non-optimized conditions, higher CNT settings corresponded to increasingly complex and vibration-intensive trajectories, especially at CNT100 and CNT75, where vibrations significantly intensified. Conversely, under the optimized mode, regardless of CNT settings, trajectory smoothness was markedly improved, and vibration amplitudes were substantially reduced, demonstrating the clear superiority of the optimized mode, particularly at higher CNT configurations.

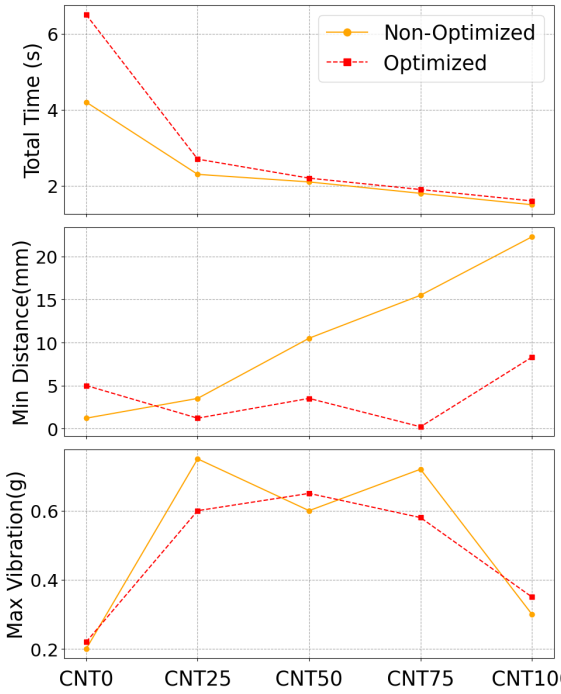

Fig. 12. Comparison between non-optimized and optimized methods under complex trajectories:(a) total execution time (b) minimum positional deviation(c) maximum vibration.

Fig. 12 further compares the total execution time, minimum positional deviation, and maximum vibration between optimized and non-optimized methods. The results clearly indicate that the

optimized mode significantly decreased total execution times, particularly at higher CNT settings, with time reductions ranging from approximately 12% to 20%. In terms of minimal positional deviation, the optimized mode demonstrated superior accuracy, particularly at the CNT100 setting, controlling positional errors within 5 mm. Although the optimized mode exhibited slightly higher maximum vibrations compared to the non-optimized mode, these vibrations remained within acceptable levels. The significant improvements in execution time and positional accuracy substantially enhanced the overall system performance, highlighting its suitability for applications demanding high precision and high-speed operations.

CONCLUSION

In this study, an integrated control strategy based on the combination of B-Spline curves and the L-BFGS-B optimization algorithm was proposed to address the vibration and trajectory distortion issues commonly encountered in high-speed robotic arm operations. The strategy systematically considers the dynamic selection and tuning of CNT and Override parameters.

(1) Traditional FINE mode provides superior positioning accuracy but typically leads to excessive vibration under high-speed and high-precision operational conditions. Conversely, the CNT mode can effectively reduce vibrations but usually at the cost of positional accuracy. The method proposed in this research achieves a suitable balance between smoothness and positional accuracy by appropriately selecting CNT and Override parameters, effectively controlling maximum vibration within the range of approximately 0.75–1.25 G and significantly reducing positional deviations. (2) Regarding trajectory planning, experimental results confirm that the number of B-Spline control points significantly affect overall performance. Specifically, introducing an optimal number of control points (e.g., two control points) substantially enhanced trajectory accuracy (reducing average deviations from 27.68 mm to 7.52 mm), while maintaining an acceptable execution time increase of approximately 0.15 s. However, adding too many control points resulted in overfitting, negatively affecting overall performance. (3) Validation experiments conducted on complex paths demonstrated robust applicability and superior performance of the proposed optimization approach in practical scenarios. Specifically, by integrating B-Spline and L-BFGS-B optimization methods, the optimized approach reduced the total execution time by approximately 12%, positional error by around 35%, and vibration differences by approximately 20% compared to the non-optimized methods. Particularly at higher CNT settings (such as CNT75 and CNT100), the optimized method achieved execution times of approximately 0.75 s and positional deviations within approximately 5 mm, exhibiting significantly enhanced performance over traditional methods. Although vibrations in the optimized method were slightly higher than those in the non-optimized methods, they remained within acceptable limits (approximately 0.8–1.0 G). The substantial improvements in accuracy and operational efficiency make this approach especially suitable for industrial applications requiring high precision and high-speed movements.

In summary, the integrated motion control method presented in this study successfully achieves an optimal balance between precision, vibration suppression, and operational efficiency, and it is applicable to various complex trajectory scenarios. Future research may extend this methodology to multi-axis collaborative robotic systems with higher degrees of freedom and integrate real-time sensory feedback and adaptive control mechanisms, further enhancing performance in dynamic environments. The outcomes of this research contribute significantly to the fields of automated manufacturing, precision machining, and robotic motion control, providing valuable practical insights for industrial applications.

ACKNOWLEDGMENTS

The authors gratefully acknowledge the financial support provided by the National Science and Technology Council (NSTC), Taiwan, under grant number NSTC 114-2222-E-167-002.

REFERENCES

Wang, W., Guo, Q., Yang, Z., Jiang, Y., and Xu, J., "A state-of-the-art review on robotic milling of complex parts with high efficiency and precision," *Robotics and Computer-Integrated Manufacturing*, 79, 102436 (2023).

Dzedzickis, A., Subačiūtė-Žemaitienė, J., Šutinys, E., Samukaitė-Bubnienė, U., and Bučinskas, V., "Advanced applications of industrial robotics: New trends and possibilities," *Applied Sciences*, Vol. 12, No. 1, 135 (2021).

Hong, T. S., Ghobakhloo, M., and Khaksar, W., "Robotic welding technology," *Comprehensive Materials Processing*, 6 (February), 77–99 (2014).

Kiran, J. S., and Prabhu, S., "Robot nano spray painting—a review," in *IOP Conference Series: Materials Science and Engineering*, Vol. 912, No. 3, p. 032044, IOP Publishing (2020, August).

Gasparetto, A., and Zanotto, V., "Optimal trajectory planning for industrial robots," *Advances in Engineering Software*, Vol. 41, No. 4, pp. 548–556 (2010).

Wang, W., Guo, Q., Yang, Z., Jiang, Y., and Xu, J., "A state-of-the-art review on robotic milling of complex parts with high efficiency and precision," *Robotics and Computer-Integrated Manufacturing*, 79, 102436 (2023).

Soori, M., Arezoo, B., and Dastres, R., "Optimization of energy consumption in industrial robots, a review," *Cognitive Robotics*, 3, pp. 142–157 (2023).

Uzuner, S., Akkus, N., and Toz, M., "Trajectory planning of a 5-DOF serial robot manipulator in joint-space," *Journal of Polytechnic-Politeknik Dergisi*, Vol. 20, No. 1, pp. 151–157 (2017).

Park, J. H., and Asada, H., "Concurrent design optimization of mechanical structure and control for high speed robots" (1994).

Zhang, T., Zhang, M., and Zou, Y., "Time-optimal and smooth trajectory planning for robot manipulators," *International Journal of Control, Automation and Systems*, Vol. 19, No. 1, pp. 521–531 (2021).

Abe, A., "An effective trajectory planning method for simultaneously suppressing residual vibration and energy consumption of flexible structures," *Case Studies in Mechanical Systems and Signal Processing*, Vol. 4, pp. 19–27 (2016).

He, H., Lu, C. L., Wen, Y., Saunders, G., Yang, P., Schoonover, J., and Wen, J. T., "High-speed high-accuracy spatial curve tracking using motion primitives in industrial robots," in *2023 IEEE International Conference on Robotics and Automation (ICRA)*, pp. 12289–12295, IEEE (2023, May).

Ratiu, M., and Prichici, M. A., "Industrial robot trajectory optimization—a review," in *MATEC Web of Conferences*, Vol. 126, p. 02005, EDP Sciences (2017).

Ziaukas, Z., Eggers, K., Kotlarski, J., and Ortmaier, T., "Optimizing PTP motions of industrial robots through addition of via-points," in *ICINCO (2)*, pp. 527–538 (2017).

He, S., Yan, C., Deng, Y., Lee, C. H., and Zhou, X., "A tolerance constrained G2 continuous path smoothing and interpolation method for industrial SCARA robots," *Robotics and Computer-Integrated Manufacturing*, 63, 101907 (2020).

Lewis, F. L., Dawson, D. M., and Abdallah, C. T., *Robot Manipulator Control: Theory and Practice*, CRC Press (2003).

Wang, H., Wang, H., Huang, J., Zhao, B., and Quan, L., "Smooth point-to-point trajectory planning for industrial robots with kinematical constraints based on high-order polynomial curve," *Mechanism and Machine Theory*, Vol. 139, pp. 284–293 (2019).

Biagiotti, L., Moriello, L., and Melchiorri, C., "Improving the accuracy of industrial robots via iterative reference trajectory modification," *IEEE Transactions on Control Systems Technology*, Vol. 28, No. 3, pp. 831–843 (2019).

Fang, Y., Hu, J., Liu, W., Shao, Q., Qi, J., and Peng, Y., "Smooth and time-optimal S-curve trajectory planning for automated robots and machines," *Mechanism and Machine Theory*, Vol. 137, pp. 127–153 (2019).

Huo, F., Zhu, S., Dong, H., and Ren, W., "A new approach to smooth path planning of Ackerman mobile robot based on improved ACO algorithm and B-spline curve," *Robotics and Autonomous Systems*, Vol. 175, 104655 (2024).

Eshtehardian, S. A., and Khodaygan, S., "A continuous RRT*-based path planning method for non-holonomic mobile robots using B-spline curves," *Journal of Ambient Intelligence and Humanized Computing*, Vol. 14, No. 7, pp. 8693–8702 (2023).

Zeng, X., and Wang, Y., "Analysis and simulation of polishing robot operation trajectory planning," *Algorithms*, Vol. 18, No. 1 (2025).

Lu, Y. A., Tang, K., and Wang, C. Y., "Collision-free and smooth joint motion planning for six-axis industrial robots by redundancy optimization," *Robotics and Computer-Integrated Manufacturing*, 68, 102091 (2021).

Ekrem, Ö., and Aksoy, B., "Trajectory planning for a 6-axis robotic arm with particle swarm optimization algorithm," *Engineering Applications of Artificial Intelligence*, Vol. 122, 106099 (2023).

Lamini, C., Benhlima, S., and Elbekri, A., "Genetic algorithm based approach for autonomous mobile robot path planning," *Procedia Computer Science*, Vol. 127, pp. 180–189 (2018).

Juříček, M., Parák, R., and Kůdela, J., "Evolutionary computation techniques for path planning problems in industrial robotics: A state-of-the-art review," *Computation*, Vol. 11, No. 12, 245 (2023).

Yamakawa, Y., Namiki, A., and Ishikawa, M., "Motion planning for dynamic knotting of a flexible rope with a high-speed robot arm," in *2010 IEEE/RSJ International Conference on Intelligent Robots and Systems*, pp. 49–54, IEEE (2010, October).

Gasparetto, A., Boscariol, P., Lanzutti, A., and Vidoni, R., "Path planning and trajectory planning algorithms: A general overview," in *Motion and Operation Planning of Robotic Systems: Background and Practical Approaches*, pp. 3–27 (2015).